International Journal of Microwave and Wireless Technologies

cambridge.org/mrf

Hyper beamforming with single-sideband time-modulated phased arrays for automotive radar

Yue Ma, Chen Miao and Wen Wu

Ministerial Key Laboratory of JGMT, Nanjing University of Science and Technology, Xiao Ling Wei200#, Nanjing 210094, China

Research Paper

Cite this article: Ma Y, Miao C, Wu W (2023). Hyper beamforming with single-sideband time-modulated phased arrays for automotive radar. *International Journal of Microwave and Wireless Technologies* **15**, 1453–1459. https://doi.org/10.1017/S175907872300017X

Received: 9 August 2022
Revised: 18 February 2023
Accepted: 21 February 2023

Keywords:
Automotive radar; hyper beamforming; narrow beamforming; time-modulated phased array

Author for correspondence:
Yue Ma,
E-mail: mayue@njust.edu.cn

Abstract

In this study, a single-sideband time-modulated phased array (STMPA)-based hyper beamforming (HBF) system for automobile radar is suggested. The left beam and the right beam are generated once the improved STMPA is split into two subarrays. The HBF method is then used to produce the hyper beam. The switching sequence may be adjusted to generate the hyper beam in the desired direction. This study's benefits may be summed up as follows: (1) The hyper beam's sidelobe level is lower and its beamwidth is narrower than the conventional beam, which can help with estimating the direction of arrival. (2) The HBF can be achieved over a very wide scanning range. (3) With time as an additional controllable variable, the system's control mode is flexible and only two channels are needed, which lowers the system's cost and complexity. The effectiveness of the algorithm is tested through simulation, and the results highlight the system's potential when used with automobile radar.

Introduction

With the development of new energy vehicles, automobile radar systems are currently the subject of intense research. In automotive systems, beamforming is crucial, particularly for communication and detection [1]. Narrow beams can be used for communication between cars in the same lane [2], or they can be used to identify numerous approaching objects [3]. Wide beams can be used for radar detection in the subsequent lane [4]. Higher angular resolution necessitates a larger array aperture because the beamwidth narrows as the array aperture grows and the beamwidth influences angular resolution. As a result, the radar volume increases, which is not ideal for some applications with constrained space. Automotive radars frequently employ Multiple Input Multiple Output (MIMO) technology because it can produce many more virtual arrays than actual arrays [3]. A better resolution in MIMO radar requires more input and output channels, which raises the cost of the system. Hyper beamforming (HBF) technology [5–9] may reduce the beamwidth in a small array aperture while also lowering the sidelobe level, in contrast to MIMO technology, which increases the virtual aperture (SLL). HBF, a type of split-beam processing technique [6], can increase direction-finding accuracy more effectively than the cross-spectrum technique [7]. It is suitable for situations with limited space, such as radar [5,8] and sonar [9]. The HBF may also be added to the system without changing the antenna layout of the array; instead, it just has to process the received signal after dividing it into the left and right subarrays, which can significantly lower the system's hardware cost. As a result, HBF is a promising method for producing focused narrow beams in automobile radar and has been shown to enhance angle resolution [5]. To the best of our knowledge, an automobile radar conventional digital beamforming system requires a separate channel for each antenna. The phased array still needs expensive installation costs and complicated feeding networks, even when HBF is used [10]. It was suggested that technology like switching beamforming networks [11] might reduce complexity and expense. This strategy, nevertheless, could result in a decrease in the beam's stability and scanning range.

Time-modulated arrays (TMA) [12] are a popular technique because of their straightforward design, which differs from conventional arrays in that they beamform utilizing radio frequency (RF) switches rather than phase shifters. Since TMA only has one output channel, signals produced by TMA are typically extracted using filters. However, a TMA's periodic modulation of the RF switches results in radiation at various harmonic frequencies, which causes energy to be lost. Therefore, harmonic suppression [13] is recommended as a means to reduce energy loss and improve TMA effectiveness. Numerous research [14–17] utilize harmonics for their flexible beamforming technique and capacity for frequency variety, as opposed to suppressing them. In a time-modulated linear array (TMLA), several beams may be easily produced in the required directions by adjusting the RF switches' on/off time [18]. Additionally, modifying the conventional TMA structure through the use of a single-

sideband time-modulated phased array (STMPA) was found to be an effective strategy [15]. Later, an upgraded STMPA (ESTMPA) was put forward [16], which strengthened the I/Q modulator's architecture. The transmission signal bandwidth was increased eight times, and the harmonic efficiency of ESTMPA reached 94.96%. When applied to the radar system, ESTMPA has a lot of promise, according to the prior studies. But the ESTMPA switching patterns should proceed through a series of equalities, producing an unmanageable sidelobe. The HBF solution is a viable approach to address the aforementioned problem. The harmonic beam operates well, according to the findings of the HBF's introduction to TMLA in [19]. In addition to successfully reducing system complexity, the dual-channel configuration is advantageous for automobile radar. Although TMLA has a traditional system structure, there remains opportunity for development in terms of performance. Comparing the ESTMPA structure to the conventional TMA structure reveals that it is more efficient and has a lower sideband level. A further benefit is the increased signal bandwidth that may be conveyed, which helps lower the filter's performance requirements. Additionally, a broader transmission signal equals greater resolution for automobile radar, which can further enhance system performance.

The current limitations of the radar and detection sensors employed in electric vehicles (EVs) include a restricted detection range and low resolution. Moreover, the costs associated with these sensors can pose a significant obstacle to their extensive adoption in the EV market. Additionally, there is an urgent need to enhance the dependability and robustness of these sensors in challenging environments and different weather conditions. The proposed scheme in this paper is based on millimeter wave band, which has good penetration for weather such as rain and fog. In addition, the system solution itself brings advantages that are expected to aid in the development of a cost-effective, high-performing sensor system for EVs, with the basic radar unit serving as the core component for accurate target detection.

According to the research above, an ESTMPA-based HBF system will offer significant benefits for enhancing the performance of the automobile radar, including narrow beamwidth, low SLL, low complexity, and broad beam scanning range. For automobile radar receivers, HBF based on the ESTMPA is suggested in this research.

System principle

Background knowledge

In an ESTMPA, as shown in Fig. 1, each antenna is connected to a reconfigurable power divider and two $0/\pi$ phase shifters, whereas one of the paths is connected to a $\pi/2$ fixed-phase shifter. The array factor of an N-element ESTMPA can be expressed as [15]

$$AF(\theta, t) = e^{j\omega_0 t} \sum_{n=0}^{N-1} I_n \cdot [U_n^I(t) + jU_n^Q(t)] \cdot e^{jKdn \sin\theta} \quad (1)$$

where $U_n^I(t)$ and $U_n^Q(t)$ are switching functions for I/Q channels. The reconfigurable power divider has two states: "One-Path-On state" and "Two-Path-On" state. In the "One-Path-On state", all energy is transferred to one channel and the other channel is closed, and $U_n^I(t) = \pm 1$, $U_n^Q(t) = \pm 1$. In the "Two-Path-On state", energy is evenly divided between the two channels, and $U_n^I(t) = \pm\sqrt{2}/2$, $U_n^Q(t) = \pm\sqrt{2}/2$. The corresponding switching sequences in the two states are shown in Fig. 2. In addition, the $0/\pi$ phase shifters can manipulate the switching sequences to be "0 states" or "π states", which control the amplitude of the sequence of positive states and negative states. $\omega_0 = 2\pi f_0$ is the angular frequency of the primary signal, $T_p = 1/f_p = 2\pi/\omega_p$ is the modulation period, I_n is the excitation amplitude of the n-th element, K is the wavenumber, and θ is the angle measured from the broad-side direction of the array. Using the Fourier transform, (1) can be written as

$$AF^{h,n} = e^{j(\omega_0 + h\omega_p)t} \sum_{n=0}^{N-1} I_n \cdot A_{h,n} \cdot e^{jKdn \sin\theta} \quad (2)$$

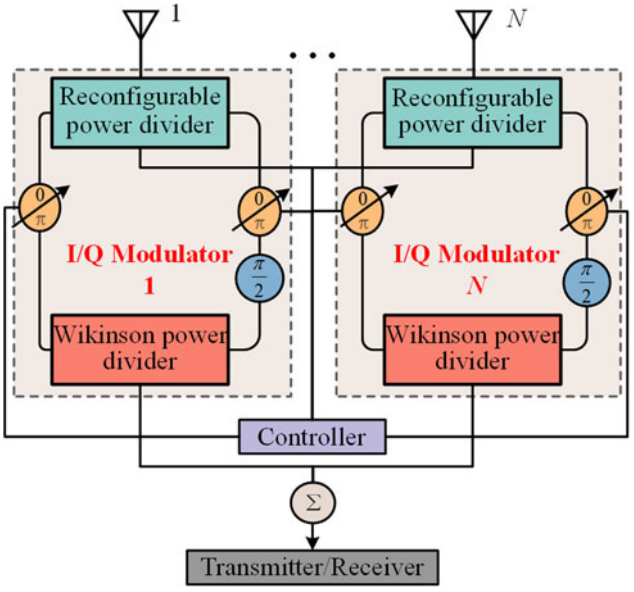

Fig. 1. The system structure of ESTMPA.

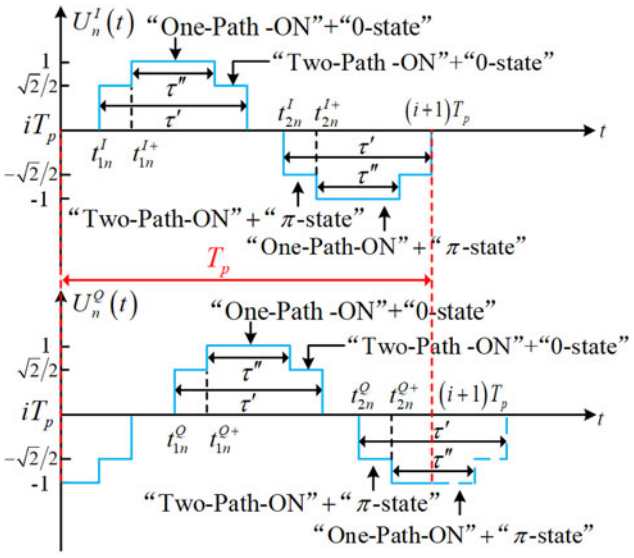

Fig. 2. The modulation waveform of $U_n^I(t)$ and $U_n^Q(t)$ in one I/Q modulator.

https://doi.org/10.1017/S175907872300017X Published online by Cambridge University Press

where h represents the number of harmonics and $A_{h,n}$ can be defined as (3)

$$A_{h,n} = \begin{cases} \frac{2}{|h|\pi}\left[\sin\left(\frac{3\pi}{8}\right) + \left(\sqrt{2}-1\right)\sin\left(\frac{\pi}{8}\right)\right] e^{-jh\pi(2t_{1n}^{I}+(1/3))}, & \text{if } h = 8k+1,\ k \in \mathbb{Z} \\ 0, \text{ others} \end{cases} \tag{3}$$

Following the rules of the switching sequences, the modulation time is shown in Fig. 2, and their relation [15] can be written as

$$\frac{\tau'}{T_p} = \frac{3}{8},\ \frac{\tau''}{T_p} = \frac{1}{8},\ \frac{t_{1n}^{Q}}{T_p} = \frac{t_{1n}^{I}}{T_p} - \frac{1}{4},\ \frac{t_{2n}^{Q} - t_{1n}^{Q}}{T_p} = \frac{t_{2n}^{I} - t_{1n}^{I}}{T_p} = \frac{1}{2} \tag{4}$$

$$\frac{t_{1n}^{I+} - t_{1n}^{I}}{T_p} = \frac{t_{2n}^{I+} - t_{2n}^{I}}{T_p} = \frac{t_{1n}^{Q+} - t_{1n}^{Q}}{T_p} = \frac{t_{2n}^{Q+} - t_{2n}^{Q}}{T_p} = \frac{\tau' - \tau''}{2T_p} \tag{5}$$

where t_{1n}^{I+}, t_{2n}^{I+}, t_{1n}^{Q+}, and t_{2n}^{Q+} represent the one-path switch-ON state starting instants, t_{1n}^{I}, t_{1n}^{Q}, t_{2n}^{I}, and t_{2n}^{Q} represent the two-path switch-ON state starting instants. Following (4) and (5), i.e. corresponding to the modulation waveform shown in Fig. 2, a considerable number of harmonics ($8k+4\pm1$, $k \in \mathrm{Z}$) in ESTMPA can be eliminated. According to equations (2) and (3), beamforming in the desired direction θ_d can be performed by designing t_{1n}^{I}, as follows

$$\frac{t_{1n}^{I}}{T_p} = \frac{nKd(\sin\theta_d)/\pi - 1/3}{2} \tag{6}$$

$$AF_r^{h,n} = \begin{cases} e^{j(\omega_0+h\omega_p)t}\sum_{n=0}^{R_N-1} I_n \cdot \frac{2}{|h|\pi}\left[\sin\left(\frac{3\pi}{8}\right) + \left(\sqrt{2}-1\right)\sin\left(\frac{\pi}{8}\right)\right] \cdot e^{-jh\pi(2t_{1n}^{I}+(1/3))} \cdot e^{jKd(n+\ (1/2))\sin\theta}, \\ \quad \text{if } h = 8k+1,\ k \in \mathbb{Z} \\ 0, \text{ others} \end{cases} \tag{7a}$$

$$AF_l^{h,n} = \begin{cases} e^{j(\omega_0+h\omega_p)t}\sum_{n=0}^{L_N-1} I_n \cdot \frac{2}{|h|\pi}\left[\sin\left(\frac{3\pi}{8}\right) + \left(\sqrt{2}-1\right)\sin\left(\frac{\pi}{8}\right)\right] \cdot e^{jh\pi(2t_{1n}^{I}+(1/3))} \cdot e^{-jKd(n+\ (1/2))\sin\theta}, \\ \quad \text{if } h = 8k+1,\ k \in \mathbb{Z} \\ 0, \text{ others} \end{cases} \tag{7b}$$

Principle of HBF in automotive radar signal processing

Figure 3 shows the HBF algorithm's basic operation and signal processing steps. As can be seen, using the beam adder and beam subtractor, the left and right beams generate sum and difference beams. The left and right beams are then modified to their c power by the beam indexer, and a beam subtracter and vector logarithm are used to generate the hyper beam for DFT/FFT. Last but not least, are the moving target detection and constant false alarm rate techniques. The proposed system differs from existing radar signal processing methods in that the received signal is processed using HBF. The hyper beam can offer improved angular resolution for future signal processing since it has a shorter beamwidth and lower sidelobe than the normal beam. As a result, the percentage of false alarms may be decreased, which is particularly beneficial for radar detection.

Figure 4 depicts the HBF block diagram of an ESTMPA-based automobile radar receiver. Two subarrays make up the ESTMPA. There are N items in each of the left and right subarrays, which are differentiated by Rn and Ln ($n = 1, 2,\ldots, N$), and the distance between them is specified as a wavelength. The left and right beams are produced by the left and right subarrays, respectively, and the array signal is obtained using two analog-to-digital converters. Additionally, signal processing and signal control may be put into practice.

The derivations are then provided. If the reference point is placed in the midst of two subarrays, then (7a) and (7b) may be used to describe the array factors of the left subarray and right subarray, correspondingly

Referring to (6), the start time of the array element in each subarray can be obtained using the following equation

$$\frac{t_{1n}^{R,I}}{T_p} = \frac{1}{2}[nKd(\sin\theta_d + 0.5)/\pi - 1/3] \tag{8a}$$

$$\frac{t_{1n}^{L,I}}{T_p} = \frac{1}{2}[-nKd(\sin\theta_d + 0.5)/\pi - 1/3] \tag{8b}$$

where $t_{1n}^{R,I}$ and $t_{1n}^{L,I}$ denote the start time of right and left subarray, respectively. Then the other switching times can be obtained

https://doi.org/10.1017/S175907872300017X Published online by Cambridge University Press

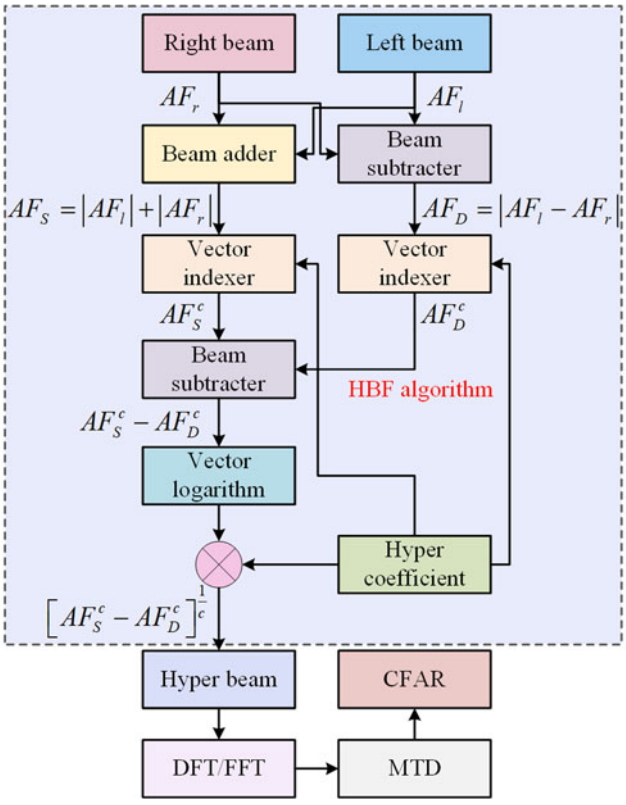

Fig. 3. The signal processing process and principle of hyper beamforming algorithm.

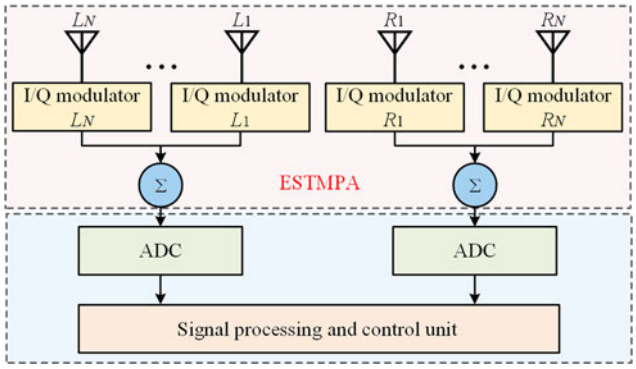

Fig. 4. Automotive radar receiver block diagram using hyper beamforming with STMPA.

according to (4) and (5). After the above formulas are obtained, the sum beam and difference beam can be obtained as

$$AF_S = |AF_l^{h,n}| + |AF_r^{h,n}| \tag{9}$$

$$AF_D = |AF_l^{h,n} - AF_r^{h,n}| \tag{10}$$

Then the hyper beam can be obtained as

$$AF_H = [AF_S^c - AF_D^c]^{1/c} \tag{11}$$

where c stands for the hyper confidence, a parameter that influences the beamwidth and sidelobe of the hyper beam and typically falls between 0.2 and 1 [20]. In the meantime, beamforming may call for maintaining a consistent beamwidth in each direction, which is very readily accomplished in HBF, as will be covered in the next subsection.

Maintain the constant beamwidth

Since the direction of beamforming may change in practice, the beamwidth can be kept constant by adjusting the confident c. The standard to split the independent beamspace is considered to be an amplitude of −3 dB of the extreme value of the beampattern, which means the following equation should be satisfied

$$AF_H|_{\theta\in[-\pi/2,\pi/2]} = \frac{AF_H|_{\theta=\theta_0}}{\sqrt{2}} \tag{12}$$

substituting (11) into (12), we can get

$$[AF_S^c - AF_D^c]^{1/c}|_{\theta\in[-\pi/2,\pi/2]} = \frac{AF_H|_{\theta=\theta_0}}{\sqrt{2}} \tag{13}$$

Through the above formula, the constant beamwidth can be guaranteed by using different c for different θ_0. For example, c varies with θ_0 as shown in Fig. 5 to keep constant beamwidth in a four-element array. As can be seen, the variation range of c is between 0.25 and 0.6 in order to maintain the beamwidth.

Numerical results

In this section, numerical experiments are simulated to verify and assess the proposed system. The primary frequency is set as f_0 = 24 GHz for potential usage in vehicle radar, and each element is scanned according to the designed switching sequences. The space between each element is set at half the wavelength. The evaluation of the proposed system includes the following points: beamforming, beamwidth, SLL, and signal transmission.

Beamforming

The suggested system's beamforming capability is implemented in this subsection. For comparison, the beam produced by ESTMPA is employed. Assume that N is 8 and that the beam direction is set in 30°. Figure 6(a) displays the hyper beam that was produced. Figures 6(b) and 6(c) demonstrate the switching patterns of the left subarray and right subarray, respectively. It can be observed

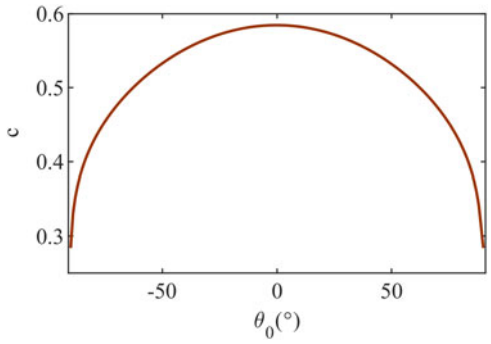

Fig. 5. The coefficient c versus θ_0 in a four-element array.

https://doi.org/10.1017/S175907872300017X Published online by Cambridge University Press

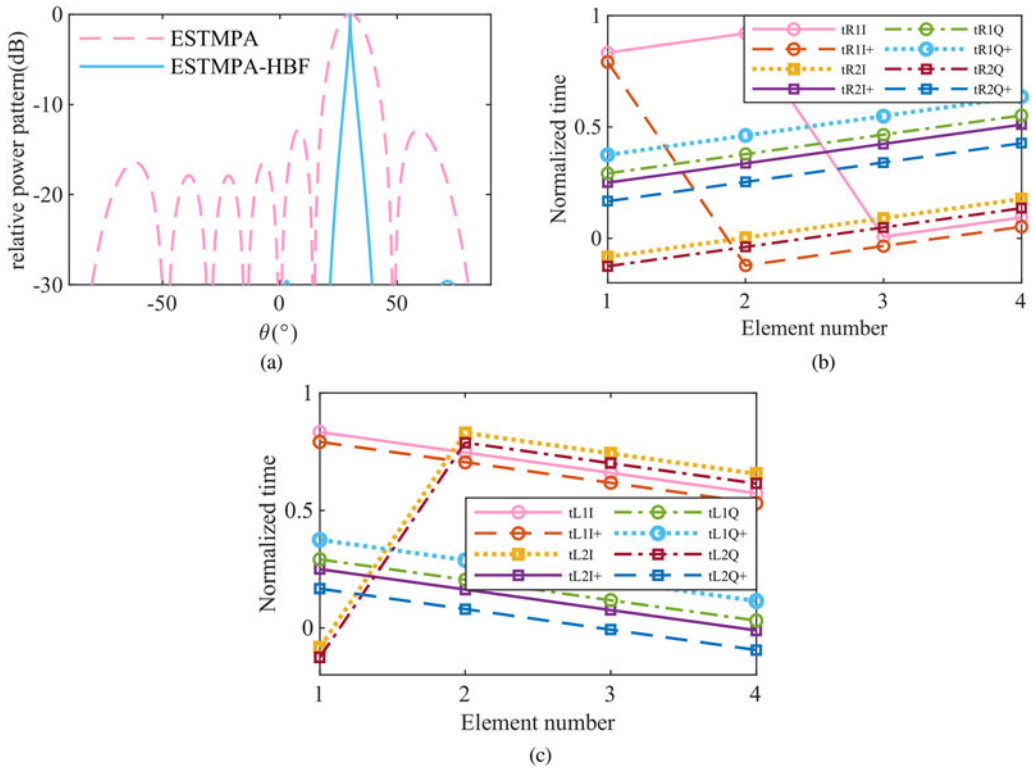

Fig. 6. (a) Radiation pattern; (b) time switching sequences of right subarray ($t1_{RX}$ denotes the switching time); (c) time switching sequences of left subarray ($t1_{LX}$ denotes the switching time).

that the hyper beam's sidelobe is smaller and its beamwidth is narrower.

Beamwidth

The beamwidth is a crucial factor to consider while evaluating the beam's performance. The suggested system is compared to the beam produced by a typical phased array. Coefficient c is the primary factor impacting the beamwidth and SLL in HBF. SLL and beamwidth may be decreased for an eight-element array, as shown in Fig. 7(a), by lowering c. Multiple incidence directions should be taken into consideration while adjusting c, due to the constant beamwidth that may be needed in practice. If *beamwidth* is fixed, the beamwidth will shrink as c increases. The lowest beamwidth, less than 0.2°, occurs when θ and c are adjusted to 0° and 0.3, as illustrated in Fig. 7(a). The beamwidth and SLL continue to grow as c rises. Figure 7(b) illustrates how c affects beamwidth. It may be observed that the beamwidth widens as c increases or as θ rises. The results of testing first null beamwidth (FNBW) and constant beamwidth performance are displayed in Table 1. It is clear that the beamwidth may be kept constant with great accuracy in each pointing direction after using (13) to modify coefficient c. Additionally, the normal beam's beamwidth is larger than the hyper beam's and varies with θ. These findings demonstrate that the hyper beam's beamwidth may be maintained constant in all directions. The FNBW, however, remains constant, indicating that the HBF approach just adds processing to the data already received and does not obtain the signal from a different source.

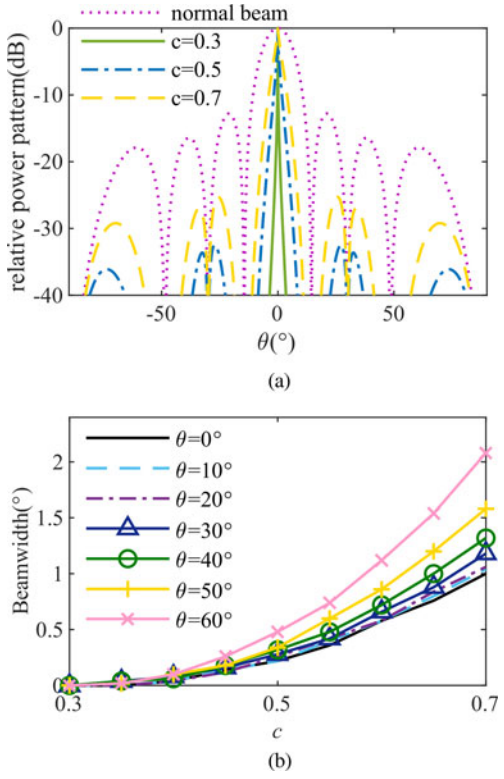

Fig. 7. (a) Radiation pattern of hyper beam with different c; (b) beamwidth versus c in different θ.

https://doi.org/10.1017/S175907872300017X Published online by Cambridge University Press

Table 1. Comparison of hyper beam and conventional beam

	Beamwidth (°)		FNBW (°)	
Incident direction (°)	Normal beam	Hyper beam	Normal beam	Hyper beam
0	12.81	1.01	28.96	28.96
10	13.02	1.01	30.14	30.14
20	13.65	1.01	32.6	32.6
30	14.85	1.01	37.2	37.2
40	16.88	1.01	46.46	46.46
50	20.48	1.01	69.21	69.21
60	28.86	1.00	79.84	79.84

SLL

SLL has a great influence on the performance of beamforming, so in this subsection, we evaluate the SLL of the system in many aspects. Figure 8(a) shows that when the number of array elements is constant, the SLL of the hyper beam is only related to c, and the influence of different incident angles on SLL is negligible. It indicates that the SLL of the hyper beam inherits very strong stability while c keeps unchanged. In addition, as the number of array elements increases, the SLL of the hyper-beam increases slightly, as shown in Fig. 8(b). This is because when the beamwidth is constant, the greater the number of array elements, the larger the value of c will be, resulting in an increase in SLL. In a practical system, a constant beam width helps to keep the performance of the system constant in each direction. When the beamwidth is constant, the SLL of the hyper-beam formed by the proposed system decreases with the increase of θ. However, compared with conventional beams, the SLL of the proposed system decreased by 13–40 dB. In practical situations, a beam with such a low SLL can guarantee the high performance of communication or radar sensing.

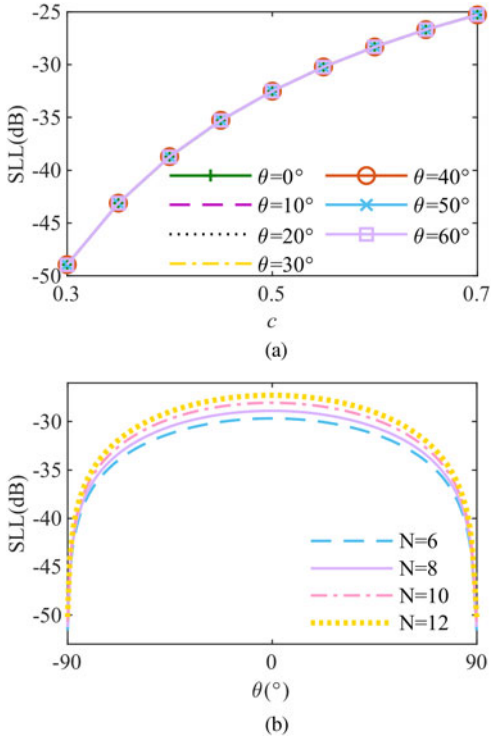

Fig. 8. (a) SLL versus c in different θ; (b) SLL versus θ with varies N.

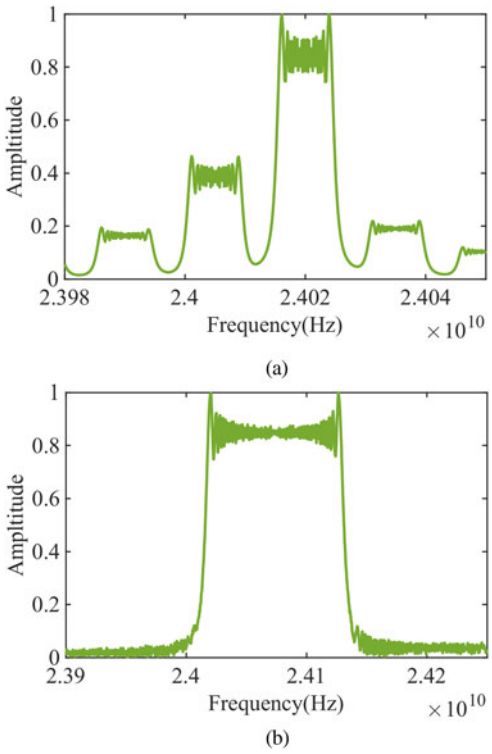

Fig. 9. LFM signal in $\theta = 10^{\circ}$ transmission by (a) traditional TMA (B = 15 MHz); (b) the proposed system (B = 120 MHz).

Signal transmission

In this subsection, a linear frequency modulation (LFM) signal is used as an example to show the advantage of ESTMPA compared to traditional TMA in signal transmission. The bandwidth of the transmitted signal cannot exceed the modulation frequency in traditional TMA. By applying ESTMPA to the automotive radar, the bandwidth of the transmitted signal can be expanded by eight times compared with the traditional TMA. Suppose a TMLA and an ESTMPA, both with eight elements, are tested in the time domain. F_p is set as 15 MHz. Figure 9 shows the comparison of the transmitted signal between the traditional TMA and ESTMPA. It can be found that ESTMPA has a larger frequency interval due to the elimination of more harmonics, which can be applied to signal transmission with higher bandwidth. Wider bandwidth means higher resolution, which will help improve the resolution of automotive radar.

Conclusion

This study proposes an HBF system for automobile radar based on ESTMPA. The left and right outputs of each subarray are used to generate the left and right beams in an ESTMPA. The HBF algorithm then produces the sum beam and difference beam before generating the hyper beam. The beam may be efficiently sharpened and the SLL decreased using the suggested

https://doi.org/10.1017/S1759078723000017X Published online by Cambridge University Press

technique. The system structure is further simplified by the usage of just two channels. Additionally, the generated beam's beamwidth may remain constant against a range of incoming angles of up to 90°, which significantly enhances and stabilizes system performance and offers an extraordinarily broad scanning range. Additionally, even if the SLL of the hyper beam will alter with angle, its maximum value is at a low level, making the SLL performance of the suggested systems appropriate for the majority of circumstances.

Overall, the suggested technique allows for narrow beamforming in a limited region while maintaining low SLL. The field of vision of the vehicle can be guaranteed by a very broad beam scanning range. Meanwhile, the straightforward design might lower system costs, making it suitable for automobile radar. Although planar arrays, cross arrays, and other types of arrays are also often employed in automobile radar, the study in this paper concentrates on the linear array. These arrays may have issues when utilized for HBF, which calls for more research in the future.

Acknowledgements. This work was supported by the National Natural Science Foundation of China No. 61671241, 62071235, 62071440, 62101258, and 62271260.

Conflict of interest. None.

References

1. **Dokhanchi SH, Mysore BS, Mishra KV and Ottersten B** (2019) A mmWave automotive joint radar-communications system. *IEEE Transactions on Aerospace and Electronic Systems* **55**, 1241–1260.
2. **Va V, Shimizu T, Bansal G and Heath RW Jr.** (2016) Millimeter wave vehicular communications: a survey. *Foundations and Trends® in Networking* **10**, 1–113.
3. **Yu Y, Hong W, Jiang ZH and Zhang H** (2020) A hybrid radar system with a phased transmitting array and a digital beamforming receiving array. *IEEE Transactions on Antennas and Propagation* **69**, 1970–1981.
4. **Patole SM, Torlak M, Wang D and Ali M** (2017) Automotive radars: a review of signal processing techniques. *IEEE Signal Processing Magazine* **34**, 22–35.
5. **Hui T and Chen M** (2019) Application of hyper beamforming algorithm in automobile anti-collision radar. In *Proc. 2019 IEEE MTT-S International Microwave Biomedical Conference (IMBioC)*, Vol. 1, pp. 1–4 (Nanjing, China), IEEE.
6. **Stergiopoulos S and Ashley AT** (1997) An experimental evaluation of split-beam processing as a broadband bearing estimator for line array sonar systems. *The Journal of the Acoustical Society of America* **102**, 3556–3563.
7. **Gou Y and Wang Y** (2011) The cross-spectrum approach for underwater multi-target direction estimation. In *Proc. 2011 International Conference of Information Technology, Computer Engineering and Management Sciences*, Vol. 2, pp. 354–357, IEEE.
8. **Lema GG, Tesfamariam GT and Mohammed MI** (2016) A novel elliptical-cylindrical antenna array for radar applications. *IEEE Transactions on Antennas and Propagation* **64**, 1681–1688.
9. **Schlieter H** (2006) Passive sonar detection improvement by hyper beam technique. *Proceedings UDT Europe*: 7A-2.
10. **Alhalabi RA and Rebeiz GM** (2014) A 77–81-GHz 16-element phased-array receiver with 50 beam scanning for advanced automotive radars. *IEEE Transaction on Microwave Theory and Techniques* **62**, 2823–2832.
11. **Djerafi T and Wu K** (2012) A low-cost wideband 77-GHz planar butler matrix in SIW technology. *IEEE Transactions on Antennas and Propagation* **60**, 4949–4954.
12. **Shanks HE and Bickmore RW** (1959) Four-dimensional electromagnetic radiators. *Canadian Journal of Physics* **37**, 263–275.
13. **Poli L, Rocca P, Manica L and Massa A** (2010) Time modulated planar arrays – analysis and optimisation of the sideband radiations. *IET Microwaves, Antennas & Propagation* **4**, 1165–1171.
14. **Ma Y, Miao C, Li YH and Wu W** (2021) A partition-based method for harmonic beamforming of time-modulated planar array. *IEEE Transactions on Antennas and Propagation* **69**, 2112–2121.
15. **Yao AM, Wu W and Fang DG** (2015) Single-sideband time-modulated phased array. *IEEE Transactions on Antennas and Propagation* **63**, 1957–1968.
16. **Chen Q, Zhang JD, Wu W and Fang DG** (2020) Enhanced single-sideband time-modulated phased array with lower sideband level and loss. *IEEE Transactions on Antennas and Propagation* **68**, 275–286.
17. **Ma Y, Miao C, Li YH and Wu W** (2021) Harmonic beamforming based on modified single-sideband time modulated phased array and its enhanced version. *IEEE Access* **9**, 57819–57828.
18. **Tong Y and Tennant A** (2010) Simultaneous control of sidelobe level and harmonic beam steering in time-modulated linear arrays. *Electronics Letters* **46**, 1.
19. **Ma Y, Miao C, Wu W and Li YH** (2020) Hyper beamforming in time modulated linear arrays. In *Proc. 2020 IEEE Asia-Pacific Microwave Conference (APMC)*, pp. 448–450 (Hong Kong, Hong Kong), IEEE.
20. **Ram G, Mandal D, Kar R and Ghosal SP** (2014) Craziness particle swarm optimization based hyper beamforming of linear antenna arrays. In *Proc. 2014 International Conference on Control, Instrumentation, Energy and Communication (CIEC)*, pp. 616–620 (Calcutta, India), IEEE.

Yue Ma received Ph.D. degree in information and communication engineering with the Nanjing University of Science and Technology, Nanjing, China in 2022. He is currently a post-doctoral fellow at Nanjing University of Science and Technology. His research interests include array signal processing and digital signal processing.

Chen Miao received the B.S., M.S., and Ph.D. degrees in electronic engineering from the Nanjing University of Science and Technology, Nanjing, China, in 2001, 2004, and 2014 respectively, where he is currently a professor with the School of Electronic Engineering and Optoelectronic Technology, Nanjing University of Science and Technology, Nanjing, China. His research interests include signal processing, microwave and millimeter-wave circuits, and detection technology.

Wen Wu received the Ph.D. degree in electromagnetic field and microwave technology from Southeast University, Nanjing, China, in 1997. He is currently a professor with the School of Electronic Engineering and Optoelectronic Technology, Nanjing University of Science and Technology, where he is also an associate director with the Ministerial Key Laboratory of JGMT. He has authored or co-authored over 300 journal and conference papers and has submitted over 30 patent applications. His current research interests include microwave and millimeter-wave theories and technologies, microwave and millimeter-wave detection, and multimode compound detection. Dr. Wu was a recipient of six times of Ministerial and Provincial-Level Science and Technology Awards.

https://doi.org/10.1017/S175907872300017X Published online by Cambridge University Press